Available online at www.sciencedirect.com
SCIENCE DIRECT®
Real-Time Imaging 11 (2005) 129–138
www.elsevier.com/locate/rti

Digital zooming for color filter array-based image sensors

Rastislav Lukac*[,1], Konstantinos N. Plataniotis

Multimedia Laboratory, BA 4157, The Edward S. Rogers Sr. Department of Electrical and Computer Engineering, University of Toronto, 10 King's College Road, Toronto, Ont., Canada M5S 3G4

Available online 23 March 2005

Abstract

In this paper, zooming methods which operate directly on color filter array (CFA) data are proposed, analyzed, and evaluated. Under the proposed framework enlarged spatial resolution images are generated directly from the CFA-based image sensors. The reduced computational complexity of the proposed schemes makes them ideal for real-time surveillance systems, industrial strength computer vision solutions, and mobile sensor-based visual systems. Simulation studies reported here indicate that the new methods (i) produce excellent results, in terms of both objective and subjective evaluation metrics, and (ii) outperform conventional zooming schemes operating in the *RGB* domain.

1. Introduction

Computer and machine vision methods are becoming increasingly important for the development and proliferation of emerging applications and commercial devices, such as wireless phones, vision-based pocket devices, sensor networks, surveillance, and automotive apparatus. Based on a single imaging sensor, usually a charge-coupled device (CCD) and complementary metal oxide semiconductor (CMOS) sensor, most solutions rely on a color filter array (CFA) to complete the image formation process [1]. Cost-effective considerations most often lead to image outputs which do not have the spatial resolution needed for subsequent vision analysis tasks, such as object recognition and scene interpretation. Therefore, digital zooming is required. It is argued here that digital zooming performed on the CFA data constitutes a promising solution that can be used to improve the performance of computer vision and robotic inspection systems, as well as that of consumer electronics and end-user camera systems.

Image formation is of paramount importance in the development of cost-effective computer vision systems [2]. Probably the most popular solutions utilize the Bayer pattern shown in Fig. 1, a CFA or mosaic of blocks formed by two green (*G*), one red (*R*) and one blue (*B*) receptors [3]. Given that a single color component is available at each spatial position, the missing color components of the captured data are interpolated from other components using the underlying spatial patterns [4–6]. This process results in restored, full color, *RGB* image. To keep cost at a reasonable level and to simultaneously increase the capturing capabilities of the sensing device, digital zooming is employed in order to increase the spatial resolution of the produced image.

In this paper, we introduce two CFA-based image zooming techniques. The methods can be seen as an extension of our initial work introduced in [7]. By operating on the CFA data directly, we avoid zooming on the *RGB* vector domain, were imperfections or noise introduced during demosaicing may create visual impairments [7,8]. Moreover, based on the proposed methods image sensor devices will directly output an enlarged *RGB* image, without the need for additional software manipulation in the *RGB* vector domain. This makes the methods attractive and useful for real-time

*Corresponding author.
E-mail address: lukacr@dsp.utoronto.ca (R. Lukac).
URL: http://www.dsp.utoronto.ca/~lukacr.
[1]Partially supported by a NATO/NSERC Science award.

1077-2014/$ - see front matter © 2005 Elsevier Ltd. All rights reserved.
doi:10.1016/j.rti.2005.01.002

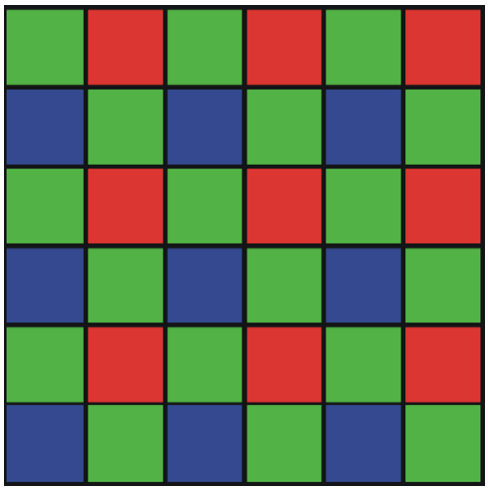

Fig. 1. Bayer CFA pattern.

image sensor applications such as mobile sensors, surveillance and computer vision systems.

The rest of this paper is organized as follows. The Bayer CFA and its fundamentals are briefly described in Section 2. The proposed framework is introduced in Section 3. Motivation and design characteristics are discussed in detail. In Section 4, the procedures under consideration are tested using a variety of images. Performance comparisons with the relevant zooming approaches are provided. Evaluation is performed, in terms of commonly used image quality measures. Complexity and implementation issues are also discussed in this section. Finally, conclusions are drawn in Section 5.

2. Fundamentals of the CFA operations

Let us consider a $K_1' \times K_2'$ Bayer image $z' : Z^2 \to Z$ depicted in Fig. 1 with $z'_{(p,q)} \in z'$ denoting the image sample (pixel) with spatial coordinates (p, q) characterizing the image row and column, respectively.

The Bayer pattern, the most widely used CFA, provides an array or mosaic of Red (R), Green (G) and Blue (B) colors in which only one color element is available at a given spatial location. In the Bayer array half of the pixels $z'_{(p,q)}$ correspond to the G channel, whereas the R, B channels are assigned the other half. By allocating more spatial samples to the Green plane, the Bayer pattern improves the perceived sharpness of the digital image since it is well-known that the human visual system (HVS) is more sensitive to luminance which is composed primarily of green light [5,9].

Given that each sample $z'_{(p,q)}$ represents a scalar value, the image data constitute a gray-scale image z' shown in Fig. 2a. However, the structure of the Bayer image is fixedly given by its spatial coordinates (p, q) and thus z' can be equivalently expressed in terms of the *RGB* vectors constituting thus a $K_1' \times K_2'$ color image $\mathbf{x}' : Z^2 \to Z^3$ shown in Fig. 2b. Assuming that $p = 1, 2, \ldots, K_1'$ and $q = 1, 2, \ldots, K_2'$ denote the spatial position (image row and column, respectively), gray-scale pixels $z'_{(p,q)}$ can be transformed into the *RGB* vectors $\mathbf{x}'_{(p,q)} = [x'_{(p,q)1}, x'_{(p,q)2}, x'_{(p,q)3}]$, using the following transformation:

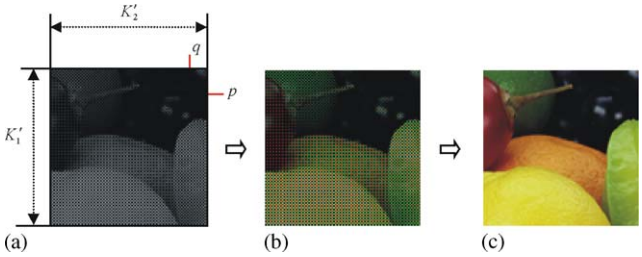

Fig. 2. CFA interpolation process: (a) original Bayer image z', (b) its corresponding color image $\mathbf{x}'$ and (c) restored color image $\mathbf{y}'$.

$$\mathbf{x}'_{(p,q)} = \begin{cases} [z'_{(p,q)}, 0, 0] & \text{for } p \text{ odd and } q \text{ even,} \\ [0, 0, z'_{(p,q)}] & \text{for } p \text{ even and } q \text{ odd,} \\ [0, z'_{(p,q)}, 0] & \text{otherwise.} \end{cases} \quad (1)$$

This transformation forms the *RGB* image representing a two-dimensional matrix of three-component samples. Note that the color vectors $\mathbf{x}'_{(p,q)}$ relate to one true component varying in m (for $m = 1, 2, 3$) of $x'_{(p,q)m}$ from position to position, whereas other two components of $\mathbf{x}'_{(p,q)}$ are set to zero. The missing color components are recovered from the adjacent Bayer data using the so-called CFA interpolation or demosaicing process [1,5,10] resulting in the restored color image shown in Fig. 2c. Bilinear interpolation (BI) is the most referred demosaicing scheme due its simplicity and robustness [11].

The BI scheme performs the interpolation step independently for each color plane. The average of the adjacent pixels is then assigned to the output [11]. The missing G components are obtained as follows:

$$x'_{(p,q)2} = \frac{1}{4} \sum_{i=1}^{4} x'_{i2}, \quad (2)$$

where $x'_{i2} \in \{x'_{(p-1,q)2}, x'_{(p,q-1)2}, x'_{(p,q+1)2}, x'_{(p+1,q)2}\}$ denotes the four neighboring G components, for $i = 1, 2, \ldots, 4$. Since the G components occupy every other position in the image rows and columns, all the missing G components of the *RGB* image $\mathbf{x}$ are interpolated using (2).

Due to the structure of the Bayer pattern and the form of the interpolator the approach for interpolating the R (or B) components is slightly different than the one used for the G components. It can be observed that only two R (or B) components are available at any corresponding G location. Therefore, at a spatial location (p, q) the R and B components are determined

as follows:

$$x'_{(p,q)m} = \frac{1}{2}\sum_{i=1}^{2} x'_{im}, \tag{3}$$

where $x'_{im} \in \{x'_{(p-1,q)m}, x'_{(p+1,q)m}\}$ or $x'_{im} \in \{x'_{(p,q-1)m}, x'_{(p,q+1)m}\}$ denote the R or B components and m is the color channel (for the R components $m = 1$, for the B components $m = 3$).

When it comes to estimate the R component at a location where a B component is available (or vice versa), it can be observed that the missing components are located at the center of four surrounding R (or B) components. Therefore, the interpolated output is given as

$$x'_{(p,q)m} = \frac{1}{4}\sum_{i=1}^{4} x'_{im}, \tag{4}$$

where $x'_{im} \in \{x'_{(p-1,q-1)m}, x'_{(p-1,q+1)m}, x'_{(p+1,q+1)m}, x'_{(p+1,q+1)m}\}$ denotes the original R and B components for $m = 1$ and 3, respectively.

Since the only operations required in the BI interpolation scheme are additions and bit shifting operations, the BI scheme is considered to be a useful, cost effective demosaicing algorithm, ideal as the baseline for performance and complexity comparisons [11]. It can be seen later that the BI's averaging approach is suitable not only for CFA interpolation, but it can be used as the base for development of CFA zooming algorithms.

3. Proposed zooming schemes

Let us consider a $K'_1 \times K'_2$ Bayer image z' depicted in Fig. 1, and spatial coordinates p, q characterizing the image row and column. Let $k \in Z$ be an arbitrary zooming factor. The value $k = 2$ is selected here to facilitate the discussion.

Zooming the Bayer image z' with a factor of k results in a $K_1 \times K_2$ zoomed Bayer image $z : Z^2 \to Z$, for $K_1 = kK'_1$ and $K_2 = kK'_2$. Conventional zooming by a factor of 2, proceeds by first enlarging the original image size and then incorporating new rows and columns (e.g. of zeros) into the original image. In the Bayer pattern, the spatial location of certain colors determine the outcome in another location. Operating on the Bayer data in this way destroys the underlying structure of the Bayer pattern as shown in Fig. 3a, since the R and B components are moved to positions (odd p, odd q) which have to correspond to the G components according to the Bayer pattern structure. It is obvious that if the pattern structure is destroyed none of the commonly used CFA demosaicing algorithms can be used to restore the full RGB color image.

To zoom the Bayer data and preserve the Bayer pattern structure, the original CFA data should be assigned unique positions in the enlarged CFA image, as shown in Figs. 3b and c. The approach depicted in Fig. 3b interleaves two new rows and columns to the sensor data. Although this step is easy to implement, it is not optimal for the CFA zooming operations, since it increases the spatial distances (by two empty rows and columns) between the essential G components in the enlarged pattern. Furthermore, due to the semi-periodic nature of the G components the approach introduces an uncertainty in the determination of the G zoomer's inputs. This is not the case when the proposed approach depicted in Fig. 3c is used. In this case, the original $z'_{(p,q)}$ values are filled into the zoomed image z as follows [7]:

$$\left.\begin{matrix} z_{(2p-1,2q)} \\ z_{(2p,2q-1)} \\ z_{(2p-1,2q-1)} \end{matrix}\right\} = z'_{(p,q)} \quad \begin{matrix} \text{for } p \text{ odd and } q \text{ even,} \\ \text{for } p \text{ even and } q \text{ odd,} \\ \text{otherwise.} \end{matrix} \tag{5}$$

It can be seen that the CFA data assigned to R and B positions, and more importantly the samples assigned to essential G positions, have equal spatial distances on the image lattice and make the structure periodic. Therefore, the approach defined in (5) is used throughout the paper.

Upon completion of this step, the enlarged Bayer image z contains all original CFA data of the input Bayer image z'. Therefore, the zooming process can continue by interpolating the missing CFA data corresponding to the empty positions of z shown in Fig. 3c.

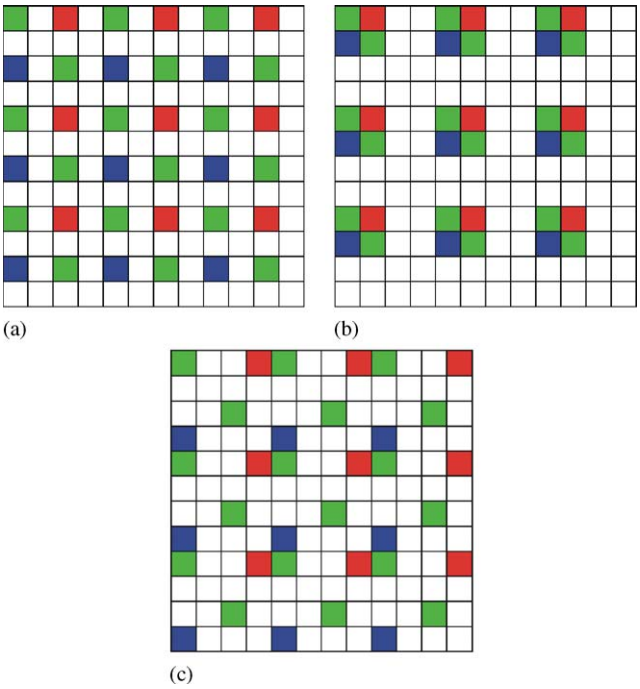

Fig. 3. Bayer pattern zooming by: (a) the standard zooming approach, which destroys the structure of the Bayer pattern (color elements do not correspond to Bayer color positions), (b) the approach interleaving two empty rows and columns and (c) the proposed method continuing in Fig. 5.

3.1. Linear averaging scheme

Since the G components are as twice as frequent (and more important for human perception) compared to R and B values, it is reasonable to continue the process by interpolating the G components corresponding to the center of a shape mask created by four surrounding values as it is shown in Fig. 4a. Using an averaging operator, the proposed linear averaging zooming scheme (LAZS) estimates the missing G CFA components of z as follows:

$$z_{(p,q)} = \frac{1}{4}\sum_{i=1}^{4} z_i, \tag{6}$$

where (p,q) denotes the spatial position in the enlarged Bayer image z, and the quantities $z_1, z_2, \ldots, z_4$ denote the four surrounding G samples $z_{(p-2,q)}$, $z_{(p,q-2)}$, $z_{(p,q+2)}$, $z_{(p+2,q)}$ forming the mask $W = \{z_1, z_2, \ldots, z_4\}$ on the image lattice (Fig. 4a). The value $z_{(p,q)}$ located at the center of the mask is set to the average of the components of W.

Using the interpolation step (6), the LAZS scheme does not introduce all the needed G components. Based on a new spatial arrangement of the G components, the rest of G components are positioned in the center of four existing G components containing original and interpolated CFA samples (Fig. 4c). Missing G components are again interpolated using (6), where $z_1, z_2, \ldots, z_4$ denote $z_{(p-1,q-1)}$, $z_{(p-1,q+1)}$, $z_{(p+1,q-1)}$, $z_{(p+1,q+1)}$. This process results in the complete set of the G components of $z(p,q)$ shown in Fig. 5a.

Interpolating the missing R and B CFA data of z is performed in the same way. It can be observed that the spatial arrangement of the original R (or B) CFA components of z also constitutes a shape mask. The missing R (or B) components are located at the mask center as it is shown in Fig. 4b. Applying the interpolation formula of (6) with $z_1, z_2, \ldots, z_4$ set to $z_{(p-2,q-2)}$, $z_{(p-2,q+2)}$, $z_{(p+2,q-2)}$, $z_{(p+2,q+2)}$, respectively; results in the formation of a new shape mask outlined in Fig. 4d. The remaining R (or B) samples are now located at the corresponding mask centers and they are interpolated by applying (6) to values $z_1, z_2, \ldots, z_4$ corresponding to $z_{(p-2,q)}$, $z_{(p,q-2)}$, $z_{(p,q+2)}$, $z_{(p+2,q)}$. This process completes the enlarged Bayer image z. The enlarged image is shown in Fig. 5b.

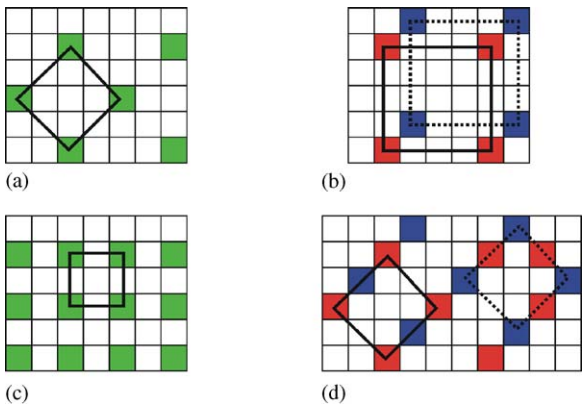

Fig. 4. Employed shape-masks for the zooming with a factor of 2: (a) a diamond-shape mask of the G components, (b) a square-shape mask of the R and B components, (c) a square-shape mask of the G components and (d) a diamond-shape mask of the R and B components.

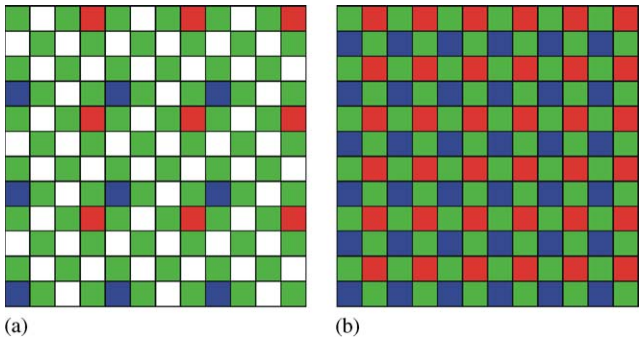

Fig. 5. Proposed zooming approach resulting in: (a) the complete G components and (b) the complete enlarged Bayer image z.

3.2. Design based on a color-difference model

Let us return to the pattern shown in Fig. 5a. This enlarged Bayer image z contains the complete set of G components. Since the G components determine, for the most part, the perceived sharpness of the digital image, it is reasonable to utilize all available G components during the R and B component calculations. In doing so, the design takes advantage of a color-difference model introduced in [12].

Comparing the location of the missing R component $z_{(p,q)}$ to the neighboring G sample $z_{(p,q-1)}$ and the locations of the four surrounding R components $z_{(p-2,q-2)}$, $z_{(p-2,q+2)}$, $z_{(p+2,q-2)}$, $z_{(p+2,q+2)}$ to the neighboring G components $z_{(p-2,q-3)}$, $z_{(p-2,q+1)}$, $z_{(p+2,q-3)}$, $z_{(p+2,q+1)}$, respectively; it is seen that all the G components have the same spatial shift. Since five G components are available compared to only four R components, instead of interpolating the missing R sample using the four R components, we decided to interpolate $z_{(p,q)}$ more accurately by combining the information provided in the available R and G samples.

The resulting scheme, called here after linear color-difference zooming (LCDZ) scheme, estimates the missing R components $z_{(p,q)}$ as

$$z_{(p,q)} = z_{(p,q-1)} + \frac{1}{4}\sum_{i=1}^{4} \bar{z}_i, \tag{7}$$

where $\bar{z}_i$ are color-difference quantities defined as follows:

$$\bar{z}_1 = z_{(p-2,q-2)} - z_{(p-2,q-3)}, \quad (8)$$

$$\bar{z}_2 = z_{(p-2,q+2)} - z_{(p-2,q+1)}, \quad (9)$$

$$\bar{z}_3 = z_{(p+2,q-2)} - z_{(p+2,q-3)}, \quad (10)$$

$$\bar{z}_4 = z_{(p+2,q+2)} - z_{(p+2,q+1)}. \quad (11)$$

Since the G component $z_{(p,q-1)}$ is available, adding the difference average value given by $\frac{1}{4}\sum_{i=1}^{4}\bar{z}_i$ guarantees the scaling of the R component output $z_{(p,q)}$.

Applying the interpolation formula of (7) for the R components, the spatial arrangement of z has been changed. Using the above difference step the pattern shown in Fig. 6a has been changed to the pattern depicted in Fig. 7a. Therefore, to complete the missing R components, the color-difference interpolation formula of (7) is defined through the difference quantities defined as follows:

$$\bar{z}_1 = z_{(p-2,q)} - z_{(p-2,q-1)}, \quad (12)$$

$$\bar{z}_2 = z_{(p,q-2)} - z_{(p,q-3)}, \quad (13)$$

$$\bar{z}_3 = z_{(p,q+2)} - z_{(p,q+1)}, \quad (14)$$

$$\bar{z}_4 = z_{(p+2,q)} - z_{(p+2,q-1)}. \quad (15)$$

Since interpolation of R and B values is basically the same process with the possible exception of the spatial coordinate indexing (Fig. 6), the color-difference interpolation formula of (7) is re-written using a simple exchange between p and q reasoned by the spatial diagonal symmetry between R and B positions. The interpolated B value is given as

$$z_{(p,q)} = z_{(p-1,q)} + \frac{1}{4}\sum_{i=1}^{4}\bar{z}_i, \quad (16)$$

where $\bar{z}_i$ are difference quantities defined as follows:

$$\bar{z}_1 = z_{(p-2,q-2)} - z_{(p-3,q-2)}, \quad (17)$$

$$\bar{z}_2 = z_{(p-2,q+2)} - z_{(p-3,q+2)}, \quad (18)$$

$$\bar{z}_3 = z_{(p+2,q-2)} - z_{(p+1,q-2)}, \quad (19)$$

$$\bar{z}_4 = z_{(p+2,q+2)} - z_{(p+1,q+2)}. \quad (20)$$

Comparing Fig. 6a and b, it can be seen that resulting R and B structures differ only in the diagonal symmetry, a fact reflected in Eqs. (7)–(11) and (16)–(20).

Analogously, applying the interpolation formula of (16), the spatial arrangement of the B values has been changed from the pattern shown in Fig. 6b to the new pattern depicted Fig. 7b. Therefore the rest of the missing B components are obtained using (16) applied to the difference quantities given as

$$\bar{z}_1 = z_{(p-2,q)} - z_{(p-3,q)}, \quad (21)$$

$$\bar{z}_2 = z_{(p,q-2)} - z_{(p-1,q-2)}, \quad (22)$$

$$\bar{z}_3 = z_{(p,q+2)} - z_{(p-1,q+2)}, \quad (23)$$

$$\bar{z}_4 = z_{(p+2,q)} - z_{(p+1,q)}. \quad (24)$$

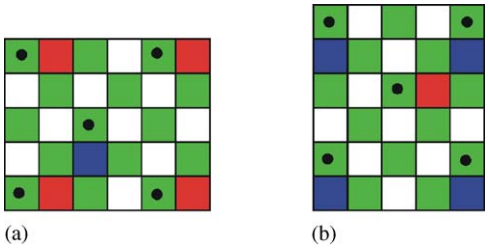

Fig. 6. Local image area corresponding to Fig. 4b: (a) for the R components and (b) for the B components.

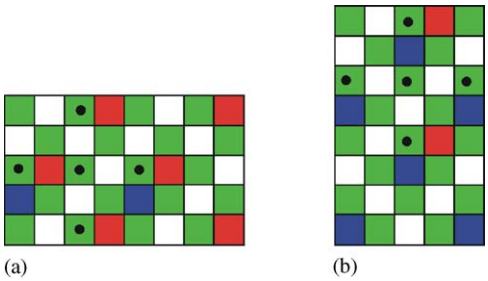

Fig. 7. Local image area corresponding to Fig. 4d: (a) for the R components and (b) for the B components.

4. Experimental results

The proposed zooming methods are tested using the color test images[1] shown in Fig. 8. These images which have been captured using professional-grade, three-sensor cameras or color scanners are being used extensively by practitioners and researchers working in camera image processing, especially in demosaicing. This is mainly due to the fact that the database contains natural, real life images which vary in complexity and color appearance. Note that in order to facilitate comparisons, all images have been normalized to the standard 512×512, 8-bit per channel RGB representation.

The efficiency of the zooming methods is measured, objectively, via the mean absolute error (MAE), the mean square error (MSE) and the normalized color difference (NCD) criterion [13]. The MAE and the MSE

[1]The used color image database is posted at the address: www.dsp.utoronto.ca/~lukacr/images8.zip

Fig. 8. Used test color images: (a) Mountains, (b) Parrots, (c) Girls and (d) Window.

criteria are defined as follows:

$$MAE = \frac{1}{3K_1K_2}\sum_{m=1}^{3}\sum_{p=1}^{K_1}\sum_{q=1}^{K_2}|o_{(p,q)m} - y_{(p,q)m}|, \tag{25}$$

$$MSE = \frac{1}{3K_1K_2}\sum_{m=1}^{3}\sum_{p=1}^{K_1}\sum_{q=1}^{K_2}(o_{(p,q)m} - y_{(p,q)m})^2, \tag{26}$$

where $\mathbf{o}_{(p,q)} = [o_{(p,q)1}, o_{(p,q)2}, o_{(p,q)3}]$ represents the original pixel, $\mathbf{y}_{(p,q)} = [y_{(p,q)1}, y_{(p,q)2}, y_{(p,q)3}]$ is the restored pixel, notation (p,q) characterizes the pixel position in a $K_1 \times K_2$ original image $\mathbf{o}$ or restored image $\mathbf{y}$ image and m characterizes the color channel.

The *NCD* criterion is given by

$$NCD = \frac{\sum_{p=1}^{K_1}\sum_{q=1}^{K_2}\sqrt{\sum_{m=1}^{3}(\bar{o}_{(p,q)m} - \bar{y}_{(p,q)m})^2}}{\sum_{p=1}^{K_1}\sum_{q=1}^{K_2}\sqrt{\sum_{m=1}^{3}(\bar{o}_{(p,q)m})^2}}, \tag{27}$$

where $\bar{\mathbf{o}}_{(p,q)} = [\bar{o}_{(p,q)1}, \bar{o}_{(p,q)2}, \bar{o}_{(p,q)3}]$ and $\bar{\mathbf{y}}_{(p,q)} = [\bar{y}_{(p,q)1}, \bar{y}_{(p,q)2}, \bar{y}_{(p,q)3}]$ are the vectors representing the *RGB* vectors $\mathbf{o}_{(p,q)}$ and $\mathbf{y}_{(p,q)}$, respectively, in the CIE LUV color space [13].

In order to apply the above criteria to $\mathbf{o}$ and $\mathbf{y}$, these images must have the same spatial resolution. Therefore, the approach shown in Fig. 9 is used. First, a $K_1 \times K_2$ original image $\mathbf{o}$ is down-sampled with a factor of k to form a $K_1' \times K_2'$ color image $\mathbf{o}'$, where $K_1 = kK_1'$ and $K_2 = kK_2'$. Since the Bayer image is usually unavailable, in order to obtain the Bayer image data used for testing and comparative evaluation, researchers resort to the approach listed in [1,5,10], where a full color image $\mathbf{o}'$ is transformed into the $K_1' \times K_2'$ Bayer image z' as follows:

$$z'_{(p,q)} = \begin{cases} o'_{(p,q)1} & \text{for } p' \text{ odd and } q' \text{ even,} \\ o'_{(p,q)3} & \text{for } p' \text{ even and } q' \text{ odd,} \\ o'_{(p,q)2} & \text{otherwise,} \end{cases} \tag{28}$$

where $\mathbf{o}'_{(p,q)} = [o'_{(p,q)1}, o'_{(p,q)2}, o'_{(p,q)3}]$ denotes the color vector in the down-sampled color image $\mathbf{o}'$ with spatial coordinates $p = 1, 2, \ldots, K_1'$ and $q = 1, 2, \ldots, K_2'$. For the original Parrots image of Fig. 9a the down-sampled color image and the corresponding Bayer image are depicted in Fig. 9b and c.

A color image $\mathbf{y}$ with dimensions $K_1 \times K_2$ can be obtained from z' by performing the conventional approach which requires to perform the BI-CFA interpolation as described in (2)–(4) followed by the conventional color image zooming (CIZ) algorithm, which employs (bi)linear interpolation [14,15]. It should

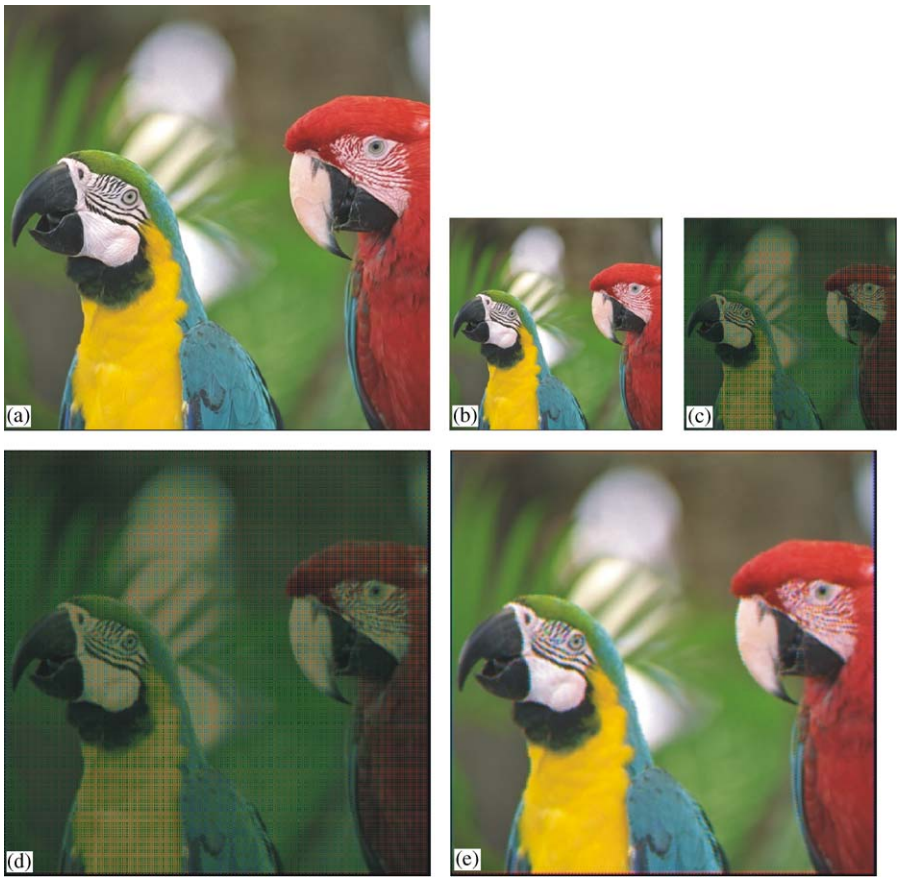

Fig. 9. Objective evaluation of the images shown in (a) and (e) obtained during the zooming process with the following steps: (a) original image **o**, (b) down-sampled image $\mathbf{o}'$, (c) color image corresponding to the Bayer image z', (d) color image corresponding to the enlarged Bayer image z achieved using the LCDZ approach and (e) restored color image **y** achieved using the BI-CFA scheme.

be emphasized that this approach performs the zooming in the *RGB* domain.

Alternatively zooming can be performed in the CFA domain. First the Bayer image z' is zoomed. This results in the enlarged Bayer image shown in Fig. 9d. A BI-CFA interpolation is then performed. This results in the $K_1 \times K_2$ color image **y** with increased spatial resolution shown in Fig. 9e. Since both approaches utilize the BI-CFA interpolation step, the proposed LASZ and LCDZ CFA zooming schemes, which operate by default on the pattern in Fig. 3c obtained via (5), can be fairly compared against the recently introduced locally adaptive CFA zooming (LAZ) scheme of Battiato [8] as well as the conventional CIZ approach. For completeness, both proposed LASZ and LCDZ approaches have also been applied to zoom the CFA image using the pattern depicted in Fig. 3b.

Tables 1–4 summarize the objective, numerical results corresponding to the test images shown in Fig. 8. Results indicate that the proposed LCDZ CFA scheme achieves the best performance in terms of MAE and MSE among all the tested zooming schemes. Therefore, it can be concluded that the employed color-difference

Table 1
Comparison of the presented algorithms using the test image Mountains

Method	*MAE*	*MSE*	*NCD*
Conventional CIZ approach	10.93	317.0	0.1701
LAZ CFA approach	11.43	352.9	0.1849
Proposed LASZ approach	11.08	320.4	0.1719
LASZ modified for Fig. 3b	12.33	399.8	0.1841
Proposed LCDZ approach	10.64	281.0	0.1932
LCDZ modified for Fig. 3b	12.18	391.4	0.1982

Table 2
Comparison of the presented algorithms using the test image Parrots

Method	*MAE*	*MSE*	*NCD*
Conventional CIZ approach	4.98	127.6	0.0374
LAZ CFA approach	5.81	158.9	0.0481
Proposed LASZ approach	5.25	137.1	0.0406
LASZ modified for Fig. 3b	6.34	178.9	0.0449
Proposed LCDZ approach	4.71	105.8	0.0418
LCDZ modified for Fig. 3b	6.11	173.9	0.0470

Table 3
Comparison of the presented algorithms using the test image Girls

Method	*MAE*	*MSE*	*NCD*
Conventional CIZ approach	5.84	132.4	0.0730
LAZ CFA approach	7.04	188.7	0.0903
Proposed LASZ approach	6.25	141.9	0.0825
LASZ modified for Fig. 3b	7.76	210.2	0.0870
Proposed LCDZ approach	5.38	107.5	0.0851
LCDZ modified for Fig. 3b	7.52	205.9	0.0922

Table 4
Comparison of the presented algorithms using the test image Window

Method	*MAE*	*MSE*	*NCD*
Conventional CIZ approach	7.23	155.2	0.0703
LAZ CFA approach	8.28	204.1	0.0908
Proposed LASZ approach	7.72	164.7	0.0780
LASZ modified for Fig. 3b	9.24	234.1	0.0837
Proposed LCDZ approach	6.45	118.9	0.0838
LCDZ modified for Fig. 3b	8.62	219.0	0.0863

model is useful for CFA zooming purposes and that the proposed scheme results in an enlarged color image, which has a close resemblance to the original. We can further argue that the reported values indicate that the proposed method preserves the structural content of the original images and enhances the detail-preserving capabilities of the CIZ and LAZ schemes. Evaluations based on the perceptually motivated NCD criterion indicates that the BI-CFA interpolation process amplifies the imperfections introduced by the color-difference model. Thus, a more efficient CFA interpolation scheme should be utilized at the second stage of the interpolation/zooming process combined with an edge-sensing mechanism. The use of powerful demosaicked image post-processor introduced in [16] may further boost the performance of the imaging solutions.

Filling the original CFA data using the approach of (5), the proposed CFA zooming schemes preserves the structure of the Bayer pattern. Comparisons between the proposed LASZ and LCDZ schemes show that improvements have been obtained as the result of the employed color difference model.

Corresponding zoomed parts of restored images are depicted in Fig. 10. They can be used for visual (subjective) evaluation. It can be seen that the best visual quality is obtained by zooming the image using the LCDZ method (Fig. 10e). LCDZ method produces sharp edges and results in a significantly smaller number of artifacts compared to the amount of color shifts and visual impairments included in the results obtained by CIZ and LAZ, and shown in Fig. 10b and 10c, respectively.

Fig. 11 summarizes estimation errors (difference images) obtained through the application of various zooming methods. It can be seen that LCDZ produces the smaller estimation error (shown in Fig. 11d) compared to the estimation errors produced by CIZ, LAZ and LASZ, and depicted in Figs. 11a–c, respectively.

Summarizing the results presented above, the following conclusions can be drawn:

- The proposed LCDZ method outperforms conventional color image zooming methods and the previously introduced CFA-based zooming schemes both in terms of objective and subjective evaluation methods.
- The LCDZ method uses the additional information afforded by the employed color-difference model along with the structure of the Bayer pattern to estimate missing values more accurately compared to the CIZ and LASZ methods.
- The LCDZ method, as well as other CFA-based solutions, avoid the proliferation of imperfections introduced during the demosaicing process, thus producing sharp, visually pleasing, zoomed color image.
- The LCDZ method is capable of zooming at an arbitrary zooming factor, preserving every time the underlying structure of the Bayer color data array.

Apart from the numerical behavior (actual performance) of any proposed algorithm, its computational complexity is a realistic measure of its practicality and usefulness. Therefore, the proposed methods are analyzed here in terms of normalized operations such as additions and divisions. It is evident that the three schemes (CIZ, LASZ and LCDZ) perform an averaging operation that differs only in a number of repetitions. In the case of the LCDZ scheme, due to the calculation of the terms suggested by the color-difference model in (7) and (16) additional operations are needed.

Let us considered the zooming factor k and a $K_1' \times K_2'$ (small) Bayer image z'. The zooming scheme output is always of size $(kK_1' \times kK_2')$ pixels. That suggests that $[(k^2-1)K_1'K_2']$ samples need to be interpolated. Considering only the zooming part of algorithms, the CIZ approach requires this amount of operations to be performed for each color channel. Therefore the overall number of interpolations performed is equal to $[3(k^2-1)K_1'K_2']$ interpolation steps or averages of the four components. Since each calculation of the average value requires 3 additions and a one division to be implemented, the CIZ approach has a computation cost of $[3(k^2-1)K_1'K_2']$ divisions and $[9(k^2-1)K_1'K_2']$ additions.

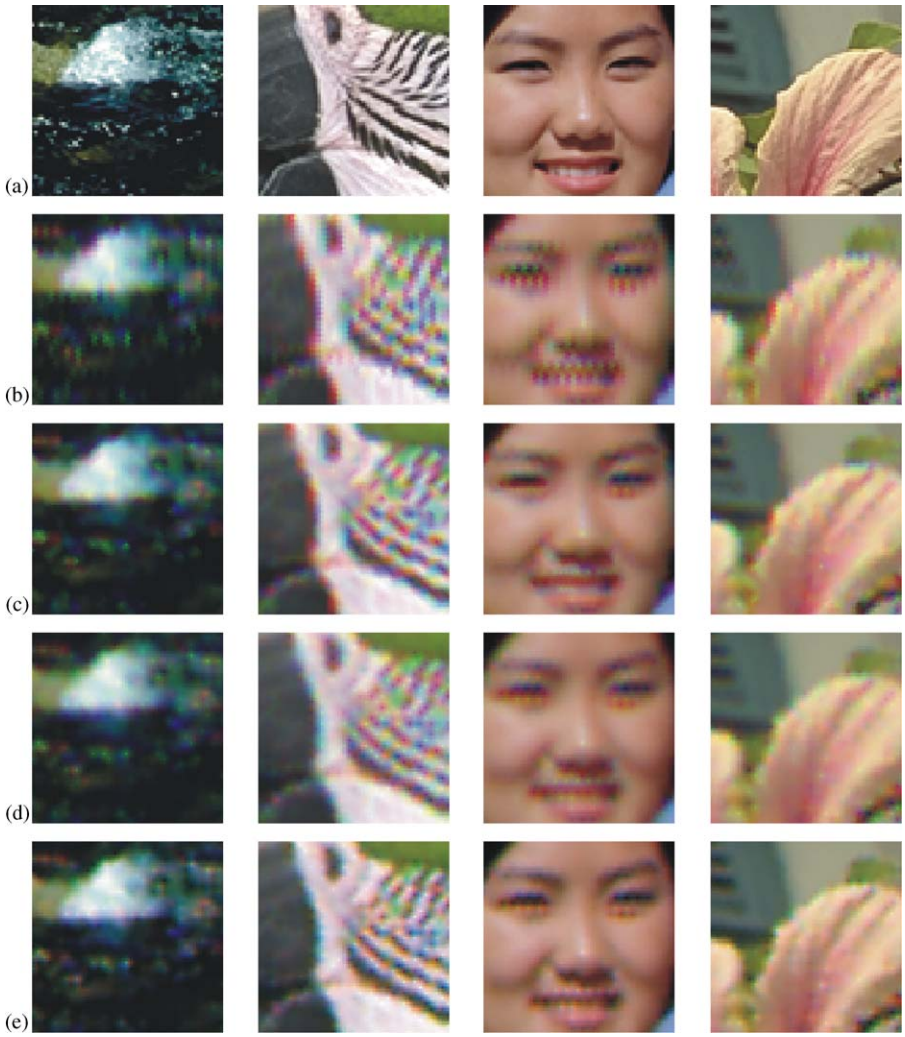

Fig. 10. Zoomed part of the results achieved using the test images shown in Fig. 8: (a) original image, (b) conventional CIZ approach, (c) LAZ CFA approach, (d) proposed LASZ CFA approach and (e) proposed LCDZ CFA approach.

In the case of the proposed LASZ approach, the algorithm operates on the Bayer data. Thus, the LASZ approach decreases the complexity three-times compared to the CIZ scheme. LASZ implementation requires $[(k^2-1)K_1'K_2']$ divisions and $[3(k^2-1)K_1'K_2']$ additions.

When evaluating the computational complexity of the LCDZ method, the difference model implementation should be taken into consideration. Since four difference quantities and one extra addition are needed to produce the final output, the LCDZ implementation requires $[8(k^2-1)K_1'K_2']$ additions and $[(k^2-1)K_1'K_2']$ divisions.

It can be therefore argued that by performing the zooming operation in the CFA domain a significant reduction in term of computational complexity can be obtained. The relative advantage increases with both the image size and the zooming factor. Therefore the proposed zooming framework is a computationally efficient method, which is useful for practical, cost-effective imaging applications.

Finally, the efficiency of the proposed zooming schemes is measured, in terms of the execution time, using a conventional PC equipped with a commonly used operating system and a standard programming environment. When implemented in software, the execution of the proposed zooming tool on a PC with an Intel Pentium IV 2.40 GHz CPU, 512 MB RAM, Windows XP operating system and MS Visual C++ 5.0 programming environment, took (on average) 0.129 and 0.146 seconds per a 256×256 pattern to be enlarged using the LASZ and LCDZ approach, respectively. The performance of the filling operations (5) took 0.015 seconds of the overall measured time. The recorded values suggest that the proposed schemes represent a computationally efficient CFA zooming solution.

Fig. 11. Estimation errors corresponding to zooming of the color images shown in Fig. 8: (a) conventional CIZ approach, (b) LAZ CFA approach, (c) proposed LASZ CFA approach and (d) proposed LCDZ CFA approach.

5. Conclusions

Two new Bayer CFA image zooming methods were introduced and analyzed. The proposed methods can be implemented using only simple operations such as additions and divisions. Extensive experimentation indicates that the proposed methods produce a sharp, visually pleasing zoomed output while at the same time they preserve the details and structural content of the original image.

References

[1] Lukac R, Plataniotis KN. Normalized color-ratio modelling for CFA interpolation. IEEE Transactions on Consumer Electronics 2004;50:737–45.
[2] Forsyth DA, Ponce J. Computer vision: a modern approach. Englewood Cliffs, NJ: Prentice-Hall; 2002.
[3] Bayer BE. Color imaging array. US Patent 3 971 065, 1976.
[4] Lukac R, Plataniotis KN, Hatzinakos D, Aleksic M. A novel cost effective demosaicing approach. IEEE Transactions on Consumer Electronics 2004;50:256–61.
[5] Gunturk B, Altunbasak Y, Mersereau R. Color plane interpolation using alternating projections. IEEE Transactions on Image Processing 2002;11:997–1013.
[6] Trussell HJ, Hartwig RE. Mathematics for demosaicking. IEEE Transactions on Image Processing 2002;11:485–92.
[7] Lukac R, Plataniotis KN. Digital camera zooming on the colour filter array. IEE Electronics Letters 2003;39:1806–7.
[8] Battiato S, Gallo G, Stanco F. A locally adaptive zooming algorithm for digital images. Image and Vision Computing 2002;20:805–12.
[9] Sharma G. Digital color imaging handbook. Boca Raton: CRC Press; 2002.
[10] Ramanath R, Snyder WE, Bilbro GL, Sander WA. Demosaicking methods for the Bayer color array. Journal of Electronic Imaging 2002;11:306–15.
[11] Longere P, Zhang X, Delahunt PB, Brainard DH. Perceptual assessment of demosaicing algorithm performance. Proceedings of the IEEE 2002;90:123–32.
[12] Adams J. Design of practical color filter array interpolation algorithms for digital cameras. Proceedings of the SPIE 1997;3028:117–25.
[13] Plataniotis KN, Venetsanopoulos AN. Color image processing and applications. Berlin: Springer; 2000.
[14] Hou HS, Andrews HC. Cubic splines for image interpolation and digital filtering. IEEE Transactions on Acoustics, Speech and Signal Processing 1978;26:508–17.
[15] Keys RG. Cubic convolution interpolation for digital image processing. IEEE Transactions on Acoustics, Speech and Signal Processing 1981;29:1153–60.
[16] Lukac R, Martin K, Plataniotis KN. Demosaicked image postprocessing using local color ratios. IEEE Transactions on Circuit and Systems for Video Technology 2004;14:914–20.